The Astrophysical Journal, 712:453–458, 2010 March 20 doi:10.1088/0004-637X/712/1/453

THREE-DIMENSIONAL POLARIMETRIC CORONAL MASS EJECTION LOCALIZATION TESTED THROUGH TRIANGULATION

Thomas G. Moran[1,2], Joseph M. Davila[3], and William T. Thompson[4]
[1] The Catholic University of America, Washington, DC 20064, USA; moran@esa.nascom.nasa.gov
[2] NASA/GSFC, Code 612.5, Greenbelt, MD 20771, USA
[3] NASA/GSFC, Code 671, Greenbelt, MD 20771, USA
[4] Adnet Systems, Inc., Lanham, MD 20771, USA
Received 2009 August 20; accepted 2010 January 28; published 2010 March 3

ABSTRACT

We have tested the validity of the coronal mass ejection (CME) polarimetric reconstruction technique for the first time using triangulation and demonstrated that it can provide the angle and distance of CMEs to the plane of the sky. In this study, we determined the three-dimensional orientation of the CMEs that occurred on 2007 August 21 and 2007 December 31 using polarimetric observations obtained simultaneously with the *Solar Terrestrial Relations Observatory*/Sun Earth Connection Coronal and Heliospheric Investigation spacecraft COR1-A and COR1-B coronagraphs. We obtained the CME orientations using both the triangulation and polarimetric techniques and found that angles to the sky plane yielded by the two methods agree to within $\approx 5^{\circ}$, validating the polarimetric reconstruction technique used to analyze CMEs observed with the *Solar and Heliospheric Observatory*/Large Angle Spectrometric Coronagraph. In addition, we located the CME source regions using EUV and magnetic field measurements and found that the corresponding mean angles to the sky plane of those regions agreed with those yielded by the geometric and polarimetric methods within uncertainties. Furthermore, we compared the locations provided by polarimetric COR1 analysis with those determined from other analyses using COR2 observations combined with geometric techniques and forward modeling. We found good agreement with those studies relying on geometric techniques but obtained results contradictory to those provided by forward modeling.

Key words: solar wind – Sun: corona – Sun: coronal mass ejections (CMEs)

1. INTRODUCTION

The violent solar eruptions known as coronal mass ejections (CMEs) can now be observed from two viewpoints simultaneously using the two separated *Solar Terrestrial Relations Observatory* (*STEREO*) spacecraft (Kaiser et al. 2008). White-light coronagraphs which are part of the *STEREO*/Sun Earth Connection Coronal and Heliospheric Investigation (SECCHI) instrument provide time-resolved polarimetric images of these eruptions in the corona (Howard et al. 2008). Polarimetric and total brightness observations can also be made from the *Solar and Heliospheric Observatory* (*SOHO*) located at L1 (Domingo et al. 1995), providing a third viewpoint. Such measurements provide information on the location and three-dimensional (3D) structure of CMEs, which is crucial for understanding the origin and dynamics of these eruptions and for predicting their effects on Earth's magnetosphere. Single-view polarimetric observations made using the Large Angle and Spectrometric Coronagraph (LASCO) on board *SOHO* (Breuckner et al. 1995) have been used to determine the 3D structure and positions of several CMEs through a technique which relies on the geometric dependence of the polarization of Thomson-scattered light (Moran & Davila 2004; Dere et al. 2005). This technique has also been employed in other studies of the 3D structure of coronal objects (Saito & Billings 1964; Crifo et al. 1983). In this method, the polarization fraction in CME emission provides a line-of-sight-averaged "mean distance to the plane of the sky" for selected or all CME pixels.

Until now there has not been an independent method to verify the 3D configuration and orientation yielded by the polarimetric technique. The launch of the two *STEREO* spacecraft, each of which carries identical polarimetric coronagraphs, has allowed a determination of 3D CME location and orientation by both polarimetric and triangulation methods. Thus, the polarimetric reconstruction technique may be tested in rigorous manner. We apply this method to two CMEs observed using the *STEREO*/SECCHI COR1 instruments to obtain 3D structural information, location, and direction of these eruptions. In addition, we determine the location and direction using triangulation from the two *STEREO* spacecraft. We find that the CME angle to the plane of the sky as determined by the polarimetric technique is consistent with that provided by the triangulation method, validating the polarimetric method. Furthermore, we compare our results with those obtained in several other studies using COR2 observations and find them to be in agreement. In addition, we determine the 3D structural details of the eruptions using the polarimetric technique. We present our observations in Section 2, our polarimetric analysis in Section 3, and our conclusions in Section 4.

2. OBSERVATIONS

On 2007 August 21, the *STEREO A* and *B* spacecraft were located 15.°0 and 11.°4 ahead and behind the Earth, respectively, at a heliocentric distance of ≈1 AU, and thus separated by 26.°4. At UT 04:45:09, a CME erupted in the SW quadrant and was detected with the SECCHI COR1-A instrument, a coronagraph which images between 1.4 $R_{\odot}$ and 4 $R_{\odot}$ through a bandpass filter 22.5 nm wide centered on the Hα line at 656 nm. A rotating polarizer is also in the beam (Thompson & Reginald 2008). Images recorded in 2048 by 2048 pixel frames at three angles separated by 60° allow measurements of total, polarized, and unpolarized brightness (Billings 1966). The total time required for a polarimetric observation sequence is ≈20 s, as compared with ≈300 s for the corresponding observation using *SOHO*/LASCO C2 (Moran & Davila 2004). The shorter exposure times

of COR1 eliminate errors arising from CME motion between exposures. Frames were binned on board to a 1024 by 1024 size, then transmitted down and binned to a 512 by 512 size to increase the signal-to-noise ratio. Pre-CME frames recorded ≈40 minutes before eruption in each of the three polarizations were subtracted from the respective CME exposures to remove stray light and non-CME coronal emission. On 2007 December 31, the *STEREO A* and *B* spacecraft were located 21.°1 ahead and 22.°6 behind the Earth, respectively, at a distance of approximately 1 AU, separated by 43.°7. At UT 01:05:09, a CME erupted in the SW quadrant and was detected with the SECCHI COR1-A instrument. Simultaneous UV observations of the solar disk and low corona were made by the SECCHI/EUVI (Howard et al. 2008) and *SOHO*/EIT (Delaboudiniere et al. 1995) instruments, and simultaneous longitudinal magnetic field measurements and white-light images were made using the *SOHO*/MDI magnetograph (Scherrer et al. 1995).

3. THREE-DIMENSIONAL POLARIMETRIC ANALYSIS OF CME STRUCTURE USING *STEREO*/SECCHI OBSERVATIONS

3.1. Structure and Location of the 2007 August 21 CME

3.1.1. EUV and Magnetograph Observations of the 2007 August 21 CME Source Region

Since the 2007 August 21 event was observed on the west limb in both A and B and was first detected in COR1-A, it was identified as a backside event. No obvious changes were observed in the SECCHI EUVI ultraviolet 195 Å images during the eruption in either A or B which would indicate the source region. However, we may determine its location from EUV observations and magnetic field measurements made several days prior to the eruption using the *STEREO*/SECCHI/EUVI, *SOHO*/EIT, and *SOHO*/MDI instruments. A UV-bright region containing multiple loops was observed in EUVI-A in the SW quadrant at UT 08:05 on 2007 August 15, centered at W60 ±5. Assuming a sidereal rotation rate of 13° per day, this would have been located at 46° ± 5° behind the *STEREO* A sky plane, which corresponds to an angle of 61° behind the Sun–Earth sky plane. The active region was also observed using *SOHO*/EIT at UT 01:03 on 2007 August 14 at 58W, which corresponds to an angle of 59° ± 5° behind the Sun–Earth sky plane. In addition, we identified the source region in a *SOHO*/MDI magnetogram recorded at UT 04:53 on 2007 August 14 as bipolar, with the neutral line oriented approximately 30° from horizontal. The region was located at W63 ±5, corresponding to an angle of 63° ± 5° behind the Earth–Sun sky plane, assuming a sidereal rotation rate of 13° per day. Therefore, the EUV and magnetic field measurements yield consistent location angles, with a mean angle of 61° ± 6°.

3.1.2. Polarimetric Analysis of the 2007 August 21 CME Structure

To obtain 3D structural information, we employ the polarimetric technique of Moran & Davila (2004). First, a table of theoretical polarized-to-unpolarized brightness ratios is computed for the relevant ranges of the scattering point radius in the plane of the sky and its distance to the plane of the sky, $|z|$, where z is the coordinate along the Earth–Sun line, using the scattering amplitude relations derived by Mineart (1930). Then, from the polarimetric COR1 observations, the plane-of-the-sky radius and polarized-to-unpolarized brightness ratio corresponding to each CME pixel are computed. To eliminate pixels with a low signal-to-noise ratio, we compute the polarization angle and omit those pixels for which it differs from tangential by more than 10°. The "mean $|z|$" value for each CME pixel is found by determining for which value of $|z|$ the measured and theoretical brightness ratios are equal. Thus, if all the mass along z were concentrated at a point, it would be located at a distance $|z|$ from the plane of the sky. The sign of z cannot be determined with this method using a single view, but EUV disk or stereoscopic observations may provide this information.

The total brightness of the CME on 2007 August 21 recorded by *STEREO*/SECCHI COR1-B at UT 11:40 is shown in Figure 1(a), and the mean $|z|$ value computed for each CME pixel using the polarimetric method and topographical (mean $|z|$) map is shown in Figure 1(d). Using the total brightness image and the topographical map, we reconstruct "top" and "side" views of the eruption under the assumption that all of the mass along the line of sight for a given pixel is concentrated at its $|z|$ value. Top and side views are shown in Figures 1(b) and 1(c), respectively. Initially, the CME appeared to be a classic three-part eruption, with a diffuse envelope and a bright, narrow inner filament. Later, as UT 11:40, this structure was less apparent. The topographical map reveals that the filament is at a greater mean angle to the plane than the envelope. Precise determination of its location from COR1-B observations is complicated by additional material along the line of sight, but COR1-A observations afforded a clear view of the filament. The total CME brightness recorded at UT 11:40 by *STEREO*/SECCHI COR1-A is shown in Figure 2(a), and the corresponding topographical map is shown in Figure 2(d). The filament as observed with COR1-A has a greater plane-of-sky extent than in COR1-B, confirming that the eruption is backside. The narrow structure expanded in a non-radial fashion, bending upward and unfolding outward. As with the COR1-B analysis, we reconstruct "top" and "side" views of the eruption, which are shown in Figures 2(b) and 2(c), respectively. A downward bending kink is present in the filament in both COR1-A and COR1-B observations, but is more apparent in A. This kink, which we use as a spatial reference, is surrounded by a box in Figure 2(a).

The COR1-A topographical map in Figure 2(d) reveals several aspects of the eruption's 3D structure. First, it is apparent that the loop-like CME is not oriented in a vertical plane; the top of the loop is at a greater plane-of-sky distance, ≈2 $R_\odot$, than the bottom, at ≈1 $R_\odot$. Second, it is apparent from the $|z|$ map that the two features near the limb at the loop bottom, at ≈150° from north measured clockwise, which appear to the base of one or more structures in the total brightness image, are not part of the same object. The upper and lower portions are at plane-of-sky angles of ≈65° and 30°, respectively. The upper portion appears to be part of the main loop-like eruption, while the lower portion, which is behind the occulter in the B images, is part of a different CME.

3.1.3. Three-dimensional Location of the 2007 August 21 CME Structure by Triangulation

The downward bending kink is indicated by arrows in Figures 3(a) and 3(b). This kink provides an independent measurement of the filament's angle from the Sun–Earth plane of the sky through triangulation. In identifying the kink, we studied multiple COR1 images of the eruption as it expanded across the frame in order to verify that the feature identified in both A and B observations was the same. Figure 4 shows lines of sight from A and B to the kink location in both instruments,

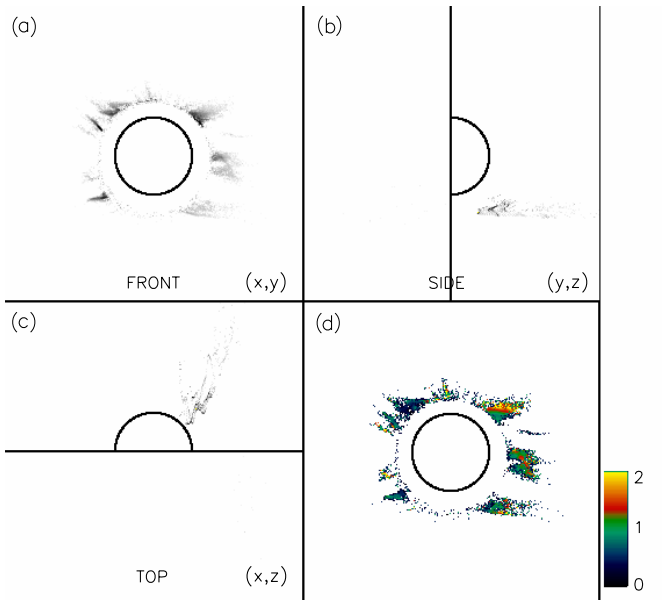

Figure 1. (a) Total brightness of the loop-like CME occurring on 2007 August 21 at 11:40 UT recorded with *STEREO*/SECCHI/COR1-B (front view), (b) a reconstructed side view of the CME in the (z, y) plane, (c) a reconstructed top view of the CME in the (x, z) plane, and (d) a topographical map of the CME displaying distance from the (x, y) plane. The color bar indicates distance from the sky plane in $R_{\odot}$. The solar disk is outlined.

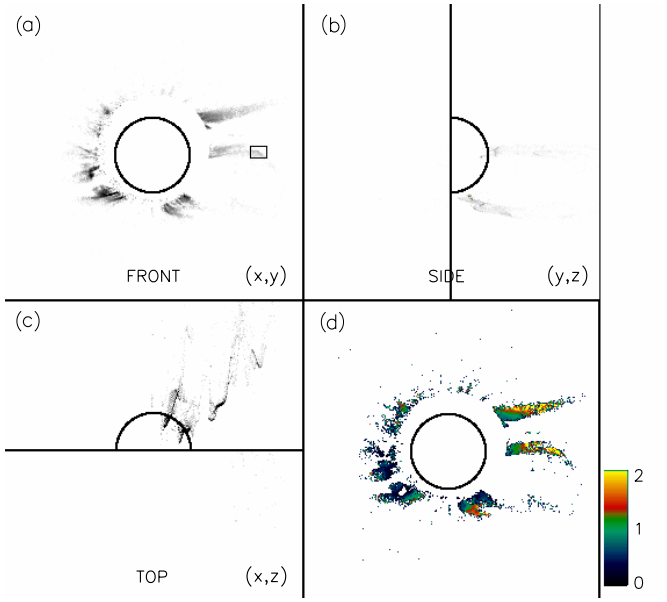

Figure 2. (a) Total brightness of the loop-like CME occurring on 2007 August 21 at 11:40 UT (front view) recorded by *STEREO*/SECCHI/COR1-A, (b) a reconstructed side view of the CME in the (z, y) plane, (c) a reconstructed top view of the CME in the (x, z) plane, and (d) a topographical map of the CME displaying distance from the (x, y) plane. The color bar indicates distance from the sky plane in $R_{\odot}$. The rectangle bounding the area containing the kink selected for localization by triangulation is shown in Figure 2(a). The solar disk is outlined.

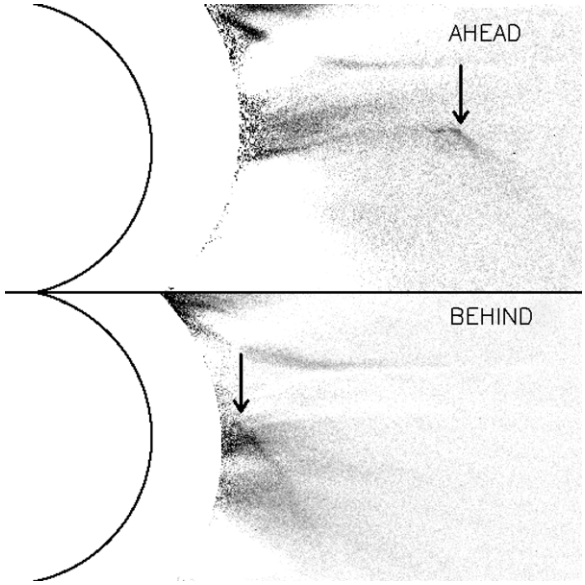

Figure 3. Image of the CME occurring on 2007 August 21 recorded at UT 11:40 in *STEREO*/SECCHI/COR1-B (upper) and *STEREO*/SECCHI/COR1-A (lower). The kink used to determine 3D CME orientation is indicated by arrows in both images.

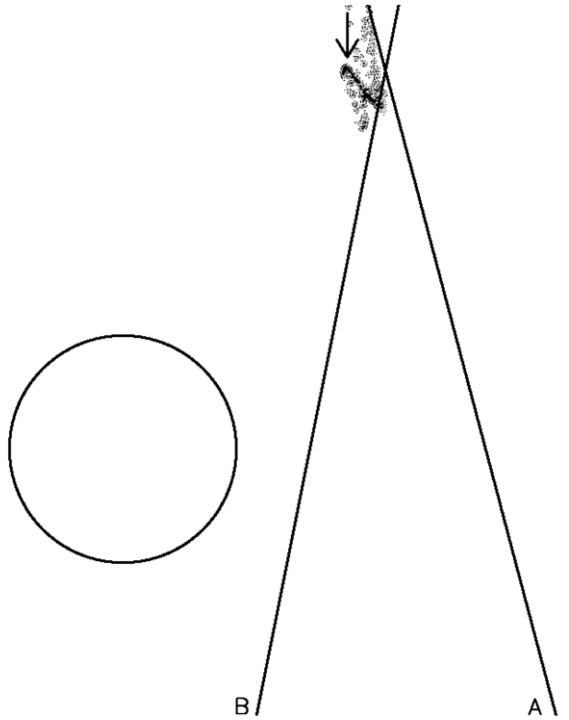

Figure 4. Top view polarimetric reconstruction in the Sun–Earth frame of the CME area bounded by the box shown in Figure 2(a). The lines of sight from COR1-A and COR1-B to the kink indicated in Figure 3 are plotted on the reconstruction. The intersection of the lines of sight yields the kink position. The kink location in the top view reconstruction is indicated by an arrow.

rotated to the Sun–Earth frame. Also shown is the top view reconstruction of the kink area observed from COR1-A, with the kink location indicated. The polarimetric reconstruction from COR1-B, contaminated by non-filament material along the line of sight, is not displayed. The sight lines intersect at the kink location, which is at an angle of 56° to the plane of the sky. The polarimetric technique yielded an angle 60° to the plane for COR1-A observations, for a relatively small difference of 4°. These results were also reported by Mierla et al. (2010). We determined the angular uncertainty in the polarimetric method to be ≈5° though noise modeling. Given the close agreement between the two methods, we find that triangulation validates the polarimetric technique. The orientation angles yielded by polarimetry and triangulation are also in approximate agreement with the position angle of the source region estimated from the

above-mentioned EUV and magnetograph disk observations made several days prior to the eruption, 61°. The difference in angle may be caused by an overestimation of the sidereal rotation rate.

The angle of the eruption was also determined geometrically from COR2-A and COR2-B observations. These coronagraphs image the corona between 2.5 $R_\odot$ and 15 $R_\odot$. Using COR-2 observation, de Koning et al. (2009) localized the CME front at 34° behind the plane of the sky, and Boursier et al. (2009) determined the CME center of mass to be 13° behind the plane. These angles are significantly different from those provided by polarimetric analysis, 60°, and from triangulation, 56°. This might be explained by errors in either of the COR1 or COR2 analyses, or by differences in location between the material selected in the investigations. Given our careful identification of the kink, we feel that the location of this material given by triangulation is correct. In order for us to obtain a plane-of-sky kink angle of 34°, we would have to place the kink at ≈0.5 $R_\odot$ further out from the location we have determined in the COR1-B image, which is not plausible. Furthermore, our location of the kink obtained through triangulation is consistent with that provided by our polarimetric analysis, and is also consistent with the position of the active region identified from disk EUV and magnetograph measurements. On the other hand, the methods used in the COR2 studies are simple and straightforward, and therefore are not likely to have errors which are large enough to explain the differences. Thus, we feel that the discrepancy between our results and those provided by the other techniques likely indicates that the filamentary kinked material located from COR1 observations using triangulation and polarimetry is separated in longitude from the outer envelope material studied in the de Koning et al. (2009) and Boursier et al. (2009) investigations by ≈22° to 51°. Apparently, the filament arose from the active region we have identified, while the outer envelope material originated to the east of its location. This indicates that the erupting filament was not centered within the overlying erupting envelope.

3.2. Structure and Location of the 2007 December 31 CME

3.2.1. EUV and Magnetograph Observations of the 2007 December 31 CME Source Region

The event was observed on the east limb in both COR1-A and COR1-B, which were separated by 44° at the time of the eruption. The CME had diffuse fronts in both views, with a plane-of-sky extent that was approximately equal in the A and B images. Owing to the diffuse nature of the front structure, triangulation cannot provide an accurate angle to the plane of the sky, but if a small longitudinal CME extent is assumed, an upper limit of the magnitude can be obtained, ≈10°. This may be compared with the EUVI-B 195 Å images recorded on 2007 December 31, showing a frontside EUV brightening in a loop-containing region near the B limb at E75 ±5 at CME initiation. The same region was observed at UT 09:35 on 2008 January 1 located at E55 ±5. These locations correspond to angles of 7.°6 ± 5° and 5.°6 ± 5° behind the Sun–Earth sky plane, respectively. The active region was also observed with *SOHO*/EIT at UT 22:00 on 2008 January 2 located at E75 ±5, corresponding to an angle of 11° ± 5° behind the Sun–Earth sky plane. In addition, the region was located in a *SOHO*/MDI magnetogram at UT 22:28 on 2008 January 2 at E60 ±5, corresponding to an angle of 8° ± 5° behind the Sun–Earth sky plane. The corresponding angles to the Sun–Earth sky plane yielded by the EUV and magnetic field measurements are consistent within uncertainties, and the mean angle to the sky plane from all of the observations was 8.°0 ± 5°. We therefore assume that the source region was located on the backside as viewed from A and the frontside as viewed from B.

3.2.2. Polarimetric Analysis of the 2007 December 31 CME Structure

The total brightness of the CME on 2007 December 31 recorded by *STEREO*/SECCHI COR1-B at UT 1:30 is shown in Figure 5(a), and the mean $|z|$ value computed for each CME pixel using the polarimetric method is shown in Figure 5(d). Reconstructed "top" and "side" views of the eruption are shown in Figures 5(b) and 5(c), respectively. The CME appears to be a classic three-part eruption, with an outer envelope and bright, inner filament. The topographical map reveals that the filament is at a greater mean angle to the B sky plane than the CME front; they appear as separate structures. The map also reveals discontinuities in mean $|z|$ both in the top and bottom regions of the eruption. We interpret the curved $|z|$ discontinuity toward the top, going from green to blue/green in the map, to be the edge of a curved cylindrical surface. The bottom contains both a smooth feature, at large angles to the plane, in orange and yellow, and a loop-like feature, in green against the orange/yellow background. Thus, the CME seems to comprise both surface-like features and distinct loops separated in longitude. These structural characteristics are not readily apparent in the total brightness image, but are clear in the topographical map.

The total CME brightness recorded at UT 1:30 by *STEREO*/SECCHI COR1-A is shown in Figure 6(a) and the corresponding topographical map is shown in Figure 6(d). Reconstructed "top" and "side" views of the eruption are shown in Figures 6(b) and 6(c), respectively. The total brightness of the front shows a similar extent in A and B, suggesting it is close to the Earth sky plane. The B topographical map reveals that the inner filament is at a distance of ≈1.5 $R_\odot$ from the sky plane, on the frontside, while it is at a distance of ≈0.75 $R_\odot$ from the A sky plane, on the backside. In addition, the top portion of the CME is frontside and ≈0.6 $R_\odot$ from the plane in B and backside and at a distance of 1.5 $R_\odot$ in A. As the view is rotated from B to A, the filament moves from frontside to backside and closer to the sky plane, while the CME top portion moved farther from the sky plane, since the filament is closer to the Earth–Sun line in longitude. The situation at the bottom region is less clear since there are both a bright loop-like feature and a wider surface-like feature separated in longitude. In both B and A topographical maps, there are regions at a range of longitudes. It is likely that the features close to the plane in B become relatively farther from the plane in A, and the structures farther from the B plane are rotated to regions relatively closer to the plane in A.

The angles to the plane of all CME points yielded by COR1-A and COR1-B observations may be compared by displaying the top views from both instruments simultaneously. Since the source region is assumed to be backside for A and frontside for B, we constructed corresponding A and B top views in each spacecraft frame. Figure 7 shows both A and B top views rotated to the Earth–Sun frame. CME pixels identified only in A or B top view reconstructions are in red or blue, respectively, while the overlap region is in green. The structures are in approximate alignment, with the A and B reconstructions at mean angles of 10.°1 and 8.°2 behind the plane of the sky, respectively, for an average angle of 9.°1 to the plane (−99.°1 measured from the Earth–Sun line). The

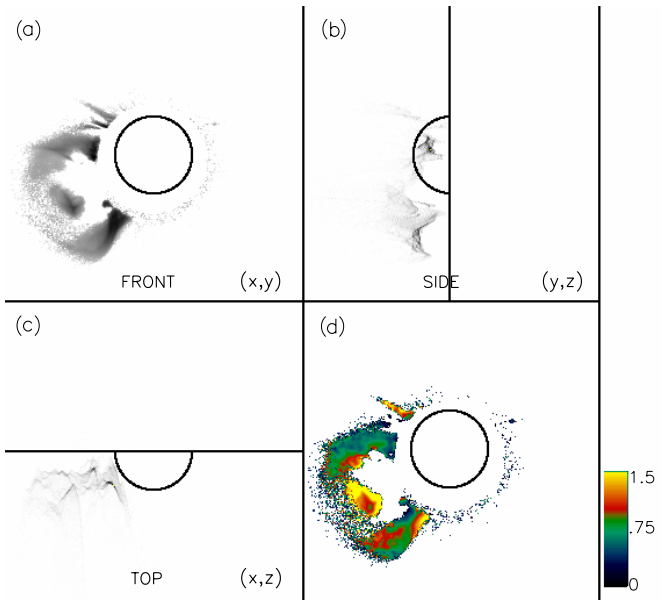

Figure 5. (a) Total brightness of the loop-like CME occurring on 2007 December 31 at 01:30 UT recorded with *STEREO*/SECCHI/COR1-B (front view), (b) a reconstructed side view of the CME in the (z, y) plane, (c) a reconstructed top view of the CME in the (x, z) plane, and (d) a topographical map of the CME displaying distance from the (x, y) plane. The color bar indicates distance from the sky plane in $R_{\odot}$. The solar disk is outlined.

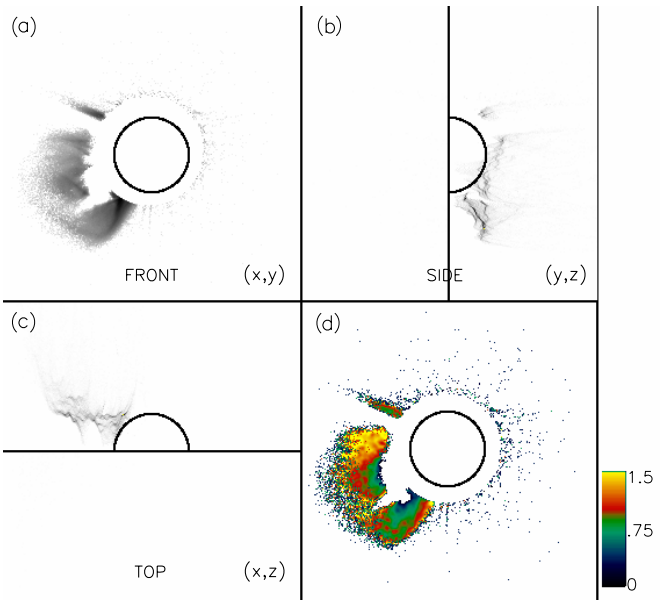

Figure 6. (a) Total brightness of the loop-like CME occurring on 2007 December 31 at 01:30 UT (front view) recorded by *STEREO*/SECCHI/COR1-A, (b) a reconstructed side view of the CME in the (z, y) plane, (c) a reconstructed top view of the CME in the (x, z) plane, and (d) a topographical map of the CME displaying distance from the (x, y) plane. The color bar indicates distance from the sky plane in $R_{\odot}$. The solar disk is outlined.

close agreement in location over most of the eruption between the polarimetric reconstructions from COR1-A and COR1-B supports the polarimetric reconstruction method. The slight misalignment between A and B might result from some material being observed in only one instrument or from some of the eruption being backside in B. The discrepancy in position close to the limb likely results from our assumption that all of the material is frontside in B and backside in A. If some of the material close to the limb in B is backside, the two reconstructions would show better agreement there. The magnitude of the angle to the plane is within the 12° upper limit determined from triangulation of the diffuse CME fronts in both spacecraft observations. In addition, the orientation angle yielded by the polarimetric method is also consistent with the location of the source region obtained from *STEREO*/SECCHI EUVI B, *SOHO*/EIT, and *SOHO*/MDI observations, which yielded a mean angle of 8°.0 (−98° measured from the Earth–Sun line) ±5° to the plane. The A and B topographical maps showed the eruption spanned at least 25° in longitude, the largest angular separation found in the maps.

The angle to the plane of this event was also determined from COR2-A and COR2-B observations. An angle of −88° for the leading edge (LE) was found using inverse reconstruction combined with forward modeling (FM; Antunes et al. 2009), −86° from triangulation of a feature on the LE (Temmer et al. 2009), −80° to −91°, from the FM of Thernisien et al. (2009), −100° from mass constraints (Colaninno & Vourlidas 2009), −94° from the geometric localization technique (de Koning et al. 2009), and −94° from tie-pointing plus triangulation of the LE (Liewer et al. 2009b). The angles provided by inverse reconstruction with FM, simple triangulation of a feature on the LE, and FM alone differ from our results by 11°, 13°, and 19° to 8°, respectively. The discrepancy between our results and those from FM may result from a mismatch between the model used in the FM and the CME's true structure. The difference between the angle provided by polarimetric analysis and that

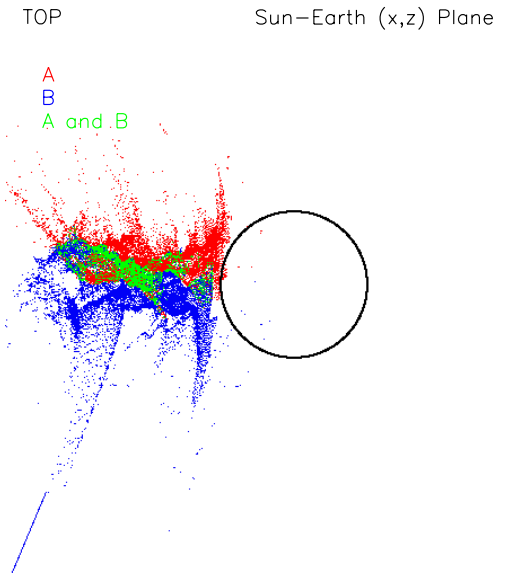

Figure 7. "Top" view of the $|z|$ locations of the 2007 December 31 CME as viewed from *STEREO*/SECCHI/COR1-A and COR1-B at UT 01:30, rotated to the Sun–Earth frame. Blue and red indicate points in the top view reconstructions made solely either from A or B observations, respectively, and green indicates the overlap region.

from simple triangulation may result from the selection of an LE feature which was separated in longitude from the eruption's center of mass. The smaller difference in the angle provided by polarimetric analysis and that provided by mass constraints, −1°, suggests that both COR2-A and COR2-B observed most of the CME's mass, which is required in order to achieve accuracy with this technique. The small angular differences between the polarimetric analysis and geometric localization, 5°, and tie-pointing plus LE triangulation, 5°, suggest that the eruption was nearly centered in the bounds used in the localization, and that

the tie-pointing plus triangulation analysis utilized a feature near the center of the eruption in longitude.

Note that a small amount of material in the COR1-B reconstruction in Figure 5 appears to be at significant angles to the Sun–Earth sky plane. This likely results from a contribution from Hα emission in the bright inner filament at the CME core. This emission results from radiative decay between the $n = 3$ and $n = 2$ levels in atomic hydrogen. Since this radiation is mostly unpolarized, and the scattering amplitude for unpolarized Thomson-scattered light peaks along the Earth–Sun line, the reconstruction algorithm returns $|z|$ values which are erroneously large if Hα emission is present.

4. CONCLUSION

Using stereoscopic observations made using the COR1-A and COR1-B coronagraphs on board the two *STEREO* spacecraft, we have demonstrated from that the single-view, polarimetric reconstruction technique used by Moran & Davila (2004) to analyze CMEs observed with *SOHO*/LASCO can alone provide the magnitude of the CME angle to the plane of the sky. The sign of the angle may be provided through stereoscopic observations or from disk observations of source regions, allowing full 3D localization. Plane-of-sky angle magnitudes of two CMEs observed stereoscopically with *STEREO*/SECCHI COR1 yielded by the polarimetric technique are consistent with those determined through triangulation, within measurement uncertainties. In addition, the CME position angles determined through polarimetry are consistent with those of the corresponding source regions identified from EUV disk observations and magnetograms. Furthermore, comparison of the locations determined from polarimetric COR1 observations with those determined from studies using total brightness COR2 observations and geometric or CME mass analyses also showed good agreement, while comparison of the our findings with those provided by FM analyses showed significant differences. Finally, the polarimetric analysis technique revealed 3D structural aspects of the 2007 December 31 CME which were not apparent from total brightness images and were consistent between the A and B observations.

This work was supported by grants from the NASA Supporting Research and Technology Program and the Living With a Star Program, and carried out at the NASA Goddard Space Flight Center *SOHO* Experimental Analyzers Facility at the NASA Goddard Space Flight Center.

REFERENCES

Antunes, A., Thernisien, A., & Yahil, A. 2009, Sol. Phys., 259, 199
Billings, B. 1966, A Guide to the Solar Corona (New York: Academic), 93
Boursier, Y., Lamy, P., & Llebaria, A. 2009, Sol. Phys., 256, 131
Breuckner, G. E., et al. 1995, Sol. Phys., 162, 357
Colaninno, R., & Vourlidas, A. 2009, ApJ, 698, 852
Crifo, F., Picat, J. P., & Cailloux, M. 1983, Sol. Phys., 83, 143
Delaboudiniere, J.-P., et al. 1995, Sol. Phys., 162, 291
de Koning, C. A., Pizzo, V. J., & Biesecker, D. A. 2009, Sol. Phys., 256, 167
Dere, K. P., Wang, D., & Howard, R. 2005, ApJ, 620, L119
Domingo, V., Fleck, B., & Poland, A. I. 1995, Sol. Phys., 162, 1
Howard, R. A., et al. 2008, Space Sci. Rev., 136, 67
Kaiser, M. L., Kucera, T. A., Davila, J. M., St. Cyr, O. C., Guhathakurta, M., & Cristian, E. 2008, Space Sci. Rev., 136, 5
Liewer, P. C., De Jong, E. M., Hall, J. R., Howard, R. A., Thompson, W. T., Culhane, J. L., Bone, L., & van Driel-Gesztelyi, L. 2009, Sol. Phys., 256, 57
Mierla, M., et al. 2010, Annal. Geophys., 28, 203
Mineart, M. 1930, Z. Astrophys., 1, 209
Moran, T. G., & Davila, J. M. 2004, Science, 305, 66
Saito, K., & Billings, D. E. 1964, ApJ, 140, 760
Scherrer, P. H., et al. 1995, Sol. Phys., 162, 129
Temmer, M., Preiss, S., & Veronig, A. M. 2009, Sol. Phys., 256, 183
Thernisien, A., Vourlidas, A., & Howard, R. A. 2009, Sol. Phys., 256, 111
Thompson, W. T., & Reginald, N. L. 2008, Sol. Phys., 250, 443